A Mobile and Self-Powered Micro-Flow Pump Based on Triboelectricity Driven Electroosmosis

Jianfeng Sun, Lingjun Zhang, Zhongjie Li, Qian Tang, Jie Chen, YingZhou Huang, Chenguo Hu, Hengyu Guo,* Yan Peng,* and Zhong Lin Wang*

Electroosmotic pumps have been widely used in microfluidic systems. However, traditional high-voltage (HV)-sources are bulky in size and induce numerous accessional reactions, which largely reduce the system's portability and efficiency. Herein, a motion-controlled, highly efficient micro-flow pump based on triboelectricity driven electroosmosis is reported. Utilizing the triboelectric nanogenerator (TENG), a strong electric field can be formed between two electrodes in the microfluidic channel with an electric double layer, thus driving the controllable electroosmotic flow by biomechanical movements. The performance and operation mechanism of this triboelectric electroosmotic pump (TEOP) is systematically studied and analyzed using a basic free-standing mode TENG. The TEOP produces ≈600 nL min^{-1} micro-flow with a Joule heat down to 1.76 J cm^{-3} nL^{-1} compared with ≈50 nL min^{-1} and 8.12 J cm^{-3} nL^{-1} for an HV-source. The advantages of economy, efficiency, portability, and safety render the TEOP a more conducive option to achieve wider applications in motion-activated micro/nanofluidic transportation and manipulation.

J. Sun, L. Zhang, Q. Tang, Prof. Y. Huang, Prof. C. Hu, Prof. H. Guo
Department of Applied Physics
State Key Laboratory of Power Transmission Equipment
and System Security and New Technology
Chongqing University
Chongqing 400044, P. R. China
E-mail: physghy@cqu.edu.cn
Prof. Z. Li, Prof. Y. Peng
School of Artificial Intelligence
Shanghai University
Shanghai 200444, P. R. China
E-mail: pengyan@shu.edu.cn
Dr. J. Chen
College of Physics and Electronic Engineering
Chongqing Normal University
Chongqing 401331, P. R. China
Prof. Z. L. Wang
Beijing Institute of Nanoenergy and Nanosystems
Chinese Academy of Sciences
Beijing 100083, P. R. China
E-mail: zhong.wang@mse.gatech.edu
Prof. Z. L. Wang
School of Materials Science and Engineering
Georgia Institute of Technology
Atlanta, GA 30332, USA

1. Introduction

The microfluidic system is an experimental platform that integrates the processes of biological/chemical/medical/environmental reactions, separation, and detection into a small chip with designed microchannels, called "lab on a chip", which has been extensively investigated and developed in many research fields.[1–11] In microfluidic systems, a micro-flow pump that drives the controllable micro-flow is the core component and shows the greatest significance.[12–14] Among various driving mechanisms, electroosmotic pumps (EOP) are widely employed in microfluidic systems due to their advantages of easy fabrication, constant fluid velocity and high integratability compared with mechanical-pressure and thermal-gradient driven approaches.[15–18] Electroosmotic pumps are usually controlled by changing the magnitude and direction of electric field in the electric double layer region that induced electroosmotic flow (EOF).[19–21] In this case, an external high-voltage (HV) DC source is mandatorily required to manipulate the EOF rate or volume, which would always form bubbles and generate Joule heat near the electrode, thus affect the efficiency of micro-flow.[22–24] Additionally, the high-voltage source is also bulk in size, high cost, and not safe,[25–27] which largely limits the miniaturization and portability of EOP-based microfluidic systems. Therefore, at this stage, facile technology to generate high voltage with economy, portability, safety, efficiency, and controllability for electroosmotic pump is highly desired.

Recently, originated from the Maxwell displacement current produced by the bound triboelectric charges,[28] triboelectric nanogenerators (TENG)[29] (Wang generators) have been developed for converting various mechanical energies into electricity with much higher efficiency in low-frequency regions (<5 Hz) to electromagnetic generators.[30] The structure of TENG device is rather simple which mainly consists of two different polymeric tribolayers with deposited electrode on the backside, and it also has abundant of materials selection according to the list of tribo-series.[31,32] These make TENGs easy to fabricate, low cost, ultraportable, and even flexible. In addition, the inherent output feature of a TENG is high voltage (≈kV) and low charge (≈nC) due to its capacitive impedance.[33] Compared with traditional HV sources, TENGs can generate a relatively safe

output voltage over 10 kV directly without complicated boosting circuits,[34] which greatly simplifies the system and have been applied for nano-electrospray ionization,[35] electrospinning,[36] micro-plasma production,[37] and negative air ion generation.[38] With these unique characters, TENG-based HV source could be a feasible technology for manipulating electroosmotic flow with the desired advantages, and for the enrichment of motion-activated microfluidic systems.

Herein, we report the first prototype of an ultraportable and motion-controlled triboelectric electroosmotic pump (TEOP) driven by a TENG. In the experiment, a free-standing (F-S)-mode TENG, which generates an open-circuit voltage of ≈35 kV and a short-circuit charge of ≈1 µC, has been employed as an HV source. The performance of producing EOF and the operation mechanism of TEOP were systematically characterized and analyzed. As a result, the sliding distance and speed of TENG controls the EOF, and the micro-flow rate and pump pressure of a single microchannel (depth: 60 µm, width: 100 µm, length: 20 mm) TEOP reaches up to ≈600 nL min^{-1} and ≈300 Pa respectively, with a low Joule heat down to 1.76 J cm^{-3} nL^{-1}. By utilizing a rotational TENG, we achieved the constant and continuous EOF, and successfully demonstrated its applications in micro-cooling system and drug transportation and mixing. The reported TEOP has great potential to contribute to the diversity of microfluidic systems in economic, portable, safe, and motion-controlled micro-flow generation.

2. Design and Characterization of the TEOP

EOPs are widely used in microfluidic systems due to their simple structure, easy integration, stable flow rate, and high controllability. However, the conventional HV source which is high in cost, complicated, bulk in size, etc., limits its diverse applications. In this work, utilizing the high output voltage of a TENG and the principle of electroosmosis, we developed the prototype of an economic, portable, efficient and motion-controlled TEOP. As the 3D schematic diagram shown in **Figure 1**a, the TEOP is a simple and portable device that mainly consists of a TENG component, a high-voltage rectifier module, and a microfluidic chip (electrode spacing 20 mm). Inset 1 shows the surface morphology of the etched tribolayer that could increase the surface charge density during electrification process and enhance the output of TENG device. For the consistency, F-S mode TENG with the size of 150 mm in length, 100 mm in width, and 8 mm in thickness was used for
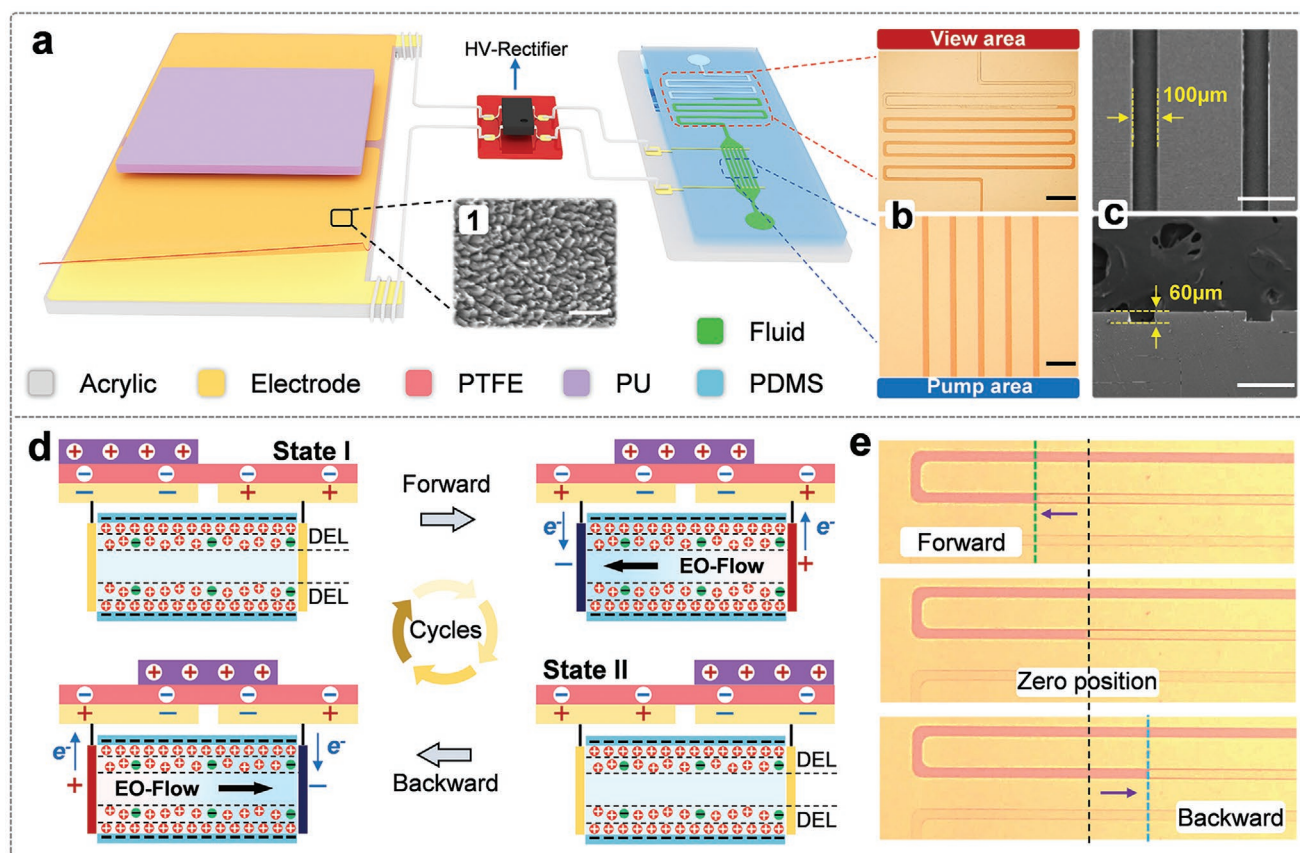

Figure 1. Prototype of the triboelectric electroosmosis pump (TEOP). a) 3D schematic diagram of the triboelectricity driven micro-flow pump composed of a TENG component, high-voltage rectifier module and microfluidic chip. Inset 1 (scale bar: 1 µm) shows the surface morphology of the tribolayer. b) Optical microscopy image of the view area (top) and pump area (bottom) in the microfluidic chip; the widths of the channels are 150 and 100 µm, respectively (scale bar: 1 mm and 500 µm). c) Electron microscopy image of the pump area; its width and height are 100 and 60 µm respectively (scale bar, 200 and 100 µm). d) The step-by-step working mechanism of the electroosmotic pump working under a full cycle of TENG movement. e) Photographs of the micro-flow while operating TENG forward and backward.

the experimental measurements. It is worth noting that, EOF can be driven by both contact-separation (C-S) mode TENG and F-S mode TENG which convert almost all kinds of mechanical energies and render the possibility of operating microfluidic systems in various occasions (e.g., utilizing outdoor energies to drive microfluidic chip for environmental detection, or harnessing biomechanical movements to activate micro-flow for drug delivery, etc.). The output of the C-S mode TENG in the separation process is much larger than that of the contact cycle (Figure S1, Supporting Information), while the output of the F-S TENG during each sliding motion is the same. Therefore, when applying the C-S mode TENG to the EOP, the flow rate for the separation process would be much greater than that of the contact process. In order to produce and characterize the TENG driven EOF, the pump area consists of several microchannels with electrode on both ends and a tortuous microchannel formed view area are designed in microfluidic chip. Figure 1b presents the optical photograph of the view area (top part) and pump area (bottom part), with the channel width of 150 and 100 μm, respectively. As the electron microscopy image shown in Figure 1c, the pump channel width is 100 μm and the height is 60 μm. The length of the pump area is determined by the distance between two electrodes which is fixed as 20 mm in our experiments. The fabrication process of the TEOP is described in detail in the Methods section and further illustrated in Figure S2, Supporting Information. The completed experimental setup is depicted in Figure S3, Supporting Information. While the fluid passing through the microchannels, an electric double layer (EDL) would be formed at the solid–liquid interface. Closed to the solid–liquid interface, there is a Stern layer with strong electrostatic adsorption that makes ions cannot move. Outside the Stern layer, there is a diffusion layer formed by the dynamic balance of positive and negative ions. As the basic mechanism of electroosmosis shown in Figure S4, Supporting Information, the net charge ions would move and drag the liquid molecules to move together under the action of external electric field, thus forming the EOF.[39,40] In Figure 1d, the F-S mode TENG was used to apply the electric field. Based on the mechanism of EOF, as the TENG sliding right from the original state I, a strong electric field to the left would be formed along the EDL channel and drives EOF in the same direction to equilibrate the potential difference. On the contrary, while TENG sliding backward from state II, EOF in a reversed direction would be produced accordingly. For verification, the obvious photographs of the liquid (deionized water) flowing forwards and backwards can be captured from the view area while operating the TENG device back and forth, as demonstrated in Figure 1e and Video S1, Supporting Information. The above preliminary results strongly proved the feasibility of a TENG-based electroosmotic pump for driving micro-flow.

3. The Basic Performance Measurement of TEOP

Commonly, an HV DC source is used to provide the driving force for EOF. To set a comparison, the basic data of EOF rate (using deionized water) and the average ion current (test by the schematic Inset of **Figure 2**a) under different applied voltages were measured and recorded before studying the performance

of TEOP. As plotted in Figure 2a, although both data points increased along with the DC voltage, the increasing rate of current was higher in the beginning and became lower afterwards than the curve slope of EOF rate. According to the mechanism of EOF described in Figure 1, there should be a linear relationship between the EOF rate and ion current. Nevertheless, as shown in Figure S5, Supporting Information, the linearity was not good when using a conventional HV source. It may be caused by some accessional chemical reactions, such as hydrolyzation, which consumes a partial electron and generates microbubbles that affect EOF. Moreover, it also leads to serious problems such as electrode erosion, and Joule heat formation.[22–24] With the fixed voltage, an HV source could provide enough charges for the reactions. In this case, the Joule heat of 8.12 J cm^{-3} nL^{-1} was yielded in the microfluidic chip under continuously 4 kV DC supply. Anyhow, from Figure 2a, nearly 1 kV was needed to drive the EOF using our designed single channel EOP efficiently. For the F-S mode TENG device used in the experiment, the maximal output open-circuit voltage and short-circuit charge of ≈35 kV and 1.2 μC was achieved under 70 mm sliding distance and 50 mm s^{-1} sliding speed as presented in Figure 2b,c respectively. Even under 20 mm sliding distance, the TENG device can also provide 4.8kV voltage output, which was high enough to drive EOF (Figure S6, Supporting Information). The output durability of TENG was also tested as shown in Figure S7, Supporting Information, which would directly affects the stability of TEOP. To characterize the performance of TEOP, the length of EOF change under different TENG sliding distance were monitored (Figure 2e and Video S2, Supporting Information), and their corresponding voltage and charge across the EOF channel were also simultaneously captured at the fixed 50 mm s^{-1} sliding speed (Figure 2d). The inset shows the schematic of the testing circuit. Noting that, the switch K was used for resetting the potential difference of two TENG electrodes at each initial state to ensure the maximized driving capability,[41] and the voltage was measured from a partial one (1 GΩ) of a serially connected resistance (600 GΩ) considering the range limitation of the electric meter. As shown in Figure 2d,e, the EOF length, voltage and charge all increased with the sliding distance of TENG increasing. Excitingly, for the 70 mm device operation, the maximum voltage reached ≈4.5 kV and EOF of nearly 14 nL in volume and 600 nL min^{-1} in rate (derived from the length change of EOF) with the generated Joule heat down to 1.76 J cm^{-3} nL^{-1} (integrated from the voltage and charge curve) was produced compared to ≈50 nL min^{-1}, 8.12 J cm^{-3} nL^{-1} for a 4 kV HV source. Furthermore, the EOF volume (EOF rate in Figure S8, Supporting Information) and transferred charge quantity with the sliding distance ranging from 20 to 70 mm were summarized and plotted in Figure 2f. From which, two diode-like curves shown a higher similarity than that in Figure 2a, and consequently, the relationship between volume and charges was also in high linearity (Inset of Figure 2f). These results indicated that, TENG driven EOP would have less side-affect reactions (generate Joule heat and bubbles) occur in EOP channel and higher efficiency than conventional HV sources. The possible mechanism maybe explained by the charge source feature of TENG device. First, the EOP chip can be regarded as a charge consumption device, in which a part of the charges across the channel could be
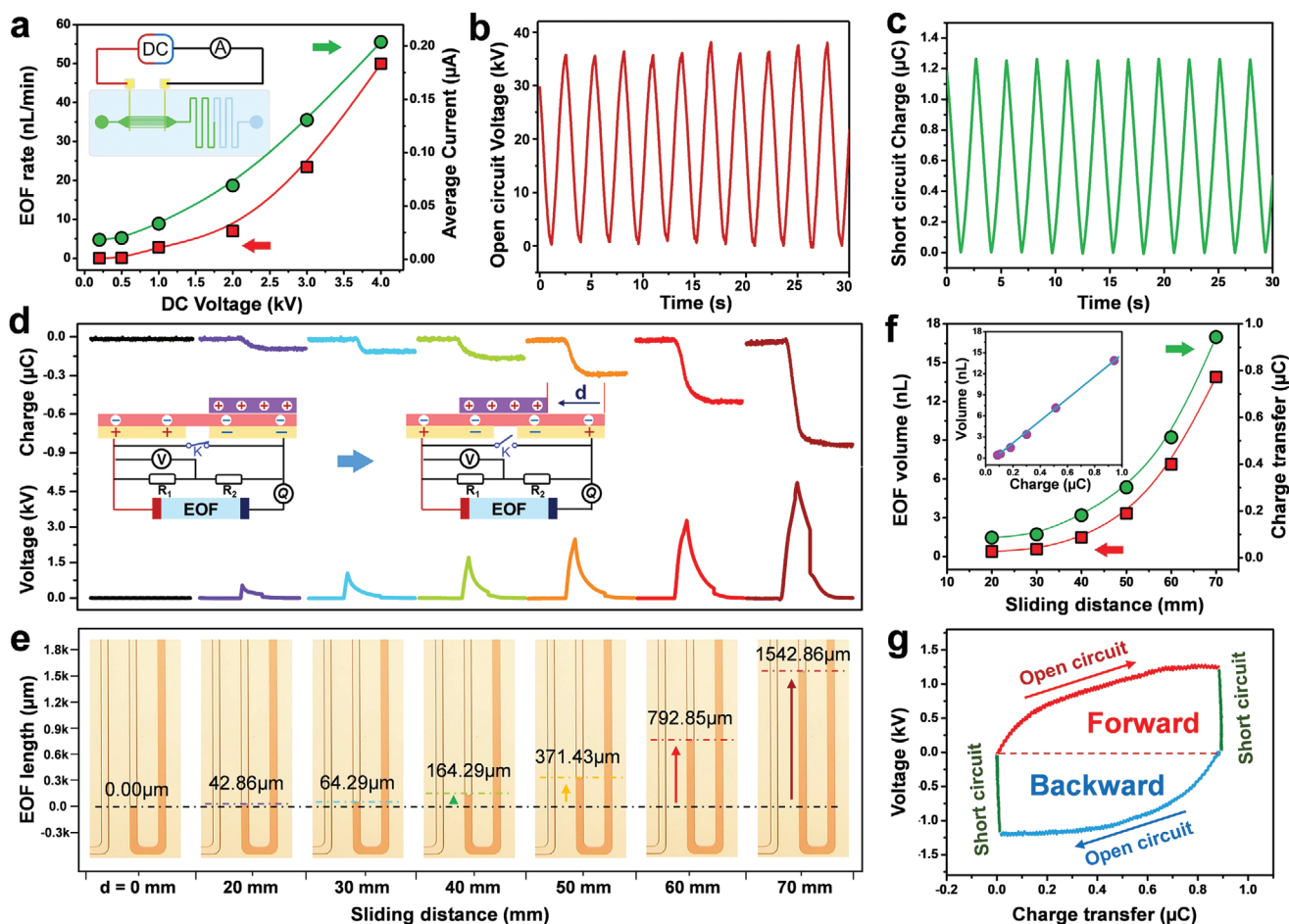
Figure 2. The performance measurement of TEOP. a) Effect of a conventional HV DC source on electroosmosis, in which, the green data indicates the relationship between the voltage and electroosmotic volume, and the red indicates the pass-through current. b,c) Open-circuit voltage and short-circuit charge of TENG (sliding distance and speed is 70 mm and 50 mm s^{-1} respectively). d) The output charge and voltage of TEOP, when increasing the sliding distance from 20 to 70 mm, and e) the corresponding created micro-flow length. f) The relationship of the TENG sliding distance on the electroosmotic flow volume and the pass-through charge quantity. Inset shows the data points between charge and flow volume (sliding distance from 20 to 70 mm). g) The V–Q curve of TEOP in one operational cycle.

converted into EOF and others would be eaten off by the accessional effect. With the applied voltage increasing, more charges are required for both parts. As discussed above, the HV source could provide sufficient charges for accessional reactions. However, for TENG device, it provides a constant charge injection rate to EOP chip and raises the voltage accordingly. Since TENG is a charge source, when more charges are needed, the voltage would stop increasing further so that to suppress the accessional reactions naturally. Figure 2g depicts the voltage–charge (V–Q) loop of a full TEOP operation cycle, as the charge injection with sliding TENG device, the voltage shown the first increasing and then saturating behavior, which could provide proofs in a certain extent. Except for the sliding distance, sliding speed also influenced the output of TENG (Figure S9, Supporting Information) and effect the performance of TEOP. As shown in Figure S10, Supporting Information, with the increase of sliding speed, the volume of EOF increased and then stabilized, while the rate of EOF increased all the time. Additionally, the influence of the EOP channel number on the electroosmotic flow volume was also studied as shown in

Figure S11, Supporting Information. Above results show that TENG is simple, portable and more efficient for driving EOF than conventional HV sources and could also precisely control the flow volume and rate by operation parameters.

4. The Pump Pressure Characterization of TEOP

Pump pressure is another important specification for a pump facility. However, the pump pressure of TEOP is too tiny to be monitored by common sensor devices, we therefore designed a home-made testing platform to quantitatively measure its pump pressure. As schematically illustrated in **Figure 3**a, a high-voltage rectifier is utilized to ensure that the direction of the electric field provided by TENG in each working cycle is constant, and a glass capillary with an inner diameter of 1 mm is sealed into the exit port of EOP chip. Considering the wicking effect, the pump pressure of TEOP can be obtained from the relatively height change of fluid column ($P = \rho g h$, where ρ represents the density of water, g is the gravitational
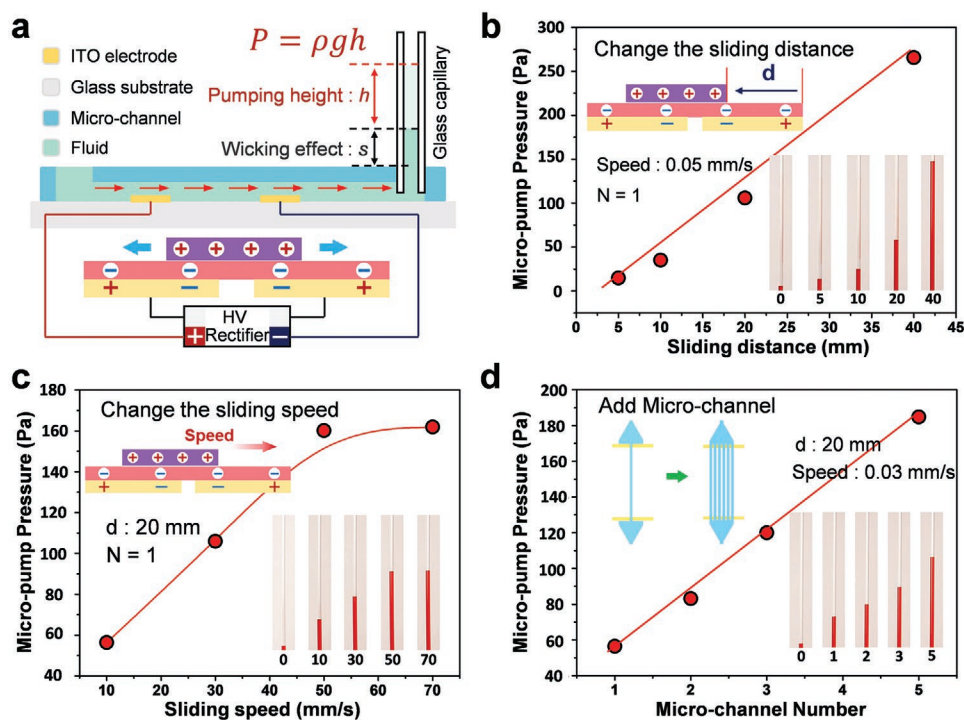
Figure 3. Characterization of the TEOP pressure. a) Schematic diagram of the testing strategy. b) The relationship between sliding distance (from 5 to 40 mm) and pump pressure for a single channel TEOP under a fixed sliding speed (50 mm s^{-1}). c) The effect of the sliding speed on the pump pressure for a single channel TEOP with a sliding distance of 20 mm. d) The pump pressure of TEOP while adding the number of microchannels (sliding speed: 30 mm s^{-1}, the sliding distance: 20 mm).

acceleration, and h is the rising height of the liquid column) between stationary state and TENG operation state. The experimental setup for pump pressure measurement is presented in Figure S12, Supporting Information. Similar to the basic performance of TEOP in Figure 2, we first studied the influence of sliding distance on the pump pressure. At a fixed sliding speed of 50 mm s^{-1}, pump pressure increased linearly with the sliding distance increasing, and reached ≈300 Pa under 40 mm sliding distance in Figure 3b. Video S3, Supporting Information demonstrated the dynamic fluid column change while varying the operation distance. In the TENG device, charges would leak or dissipate somehow, and have a dynamically balanced state with triboelectrification process which is determined by the sliding speed (Figure S9, Supporting Information). As plotted in Figure 3c, under the fixed sliding distance of 20 mm, when accelerating the speed from 10 to 70 mm s^{-1}, the pump pressure first increases and then tends to be stable. This process is also clearly shown in Video S4, Supporting Information. Finally, the relationship between pump pressure and the number of EOP channels was investigated when fixing the sliding speed and distance. The increasing of pump channels will result in the enhancement of EDL. From Figure 3d, the pump pressure linearly increased with the channel number increasing. At the same time, we also did the control experiment with a DC high-voltage source (Figure S13, Supporting Information). With the voltage increasing, the pressure of the electroosmotic pump increased to 120 Pa at 3 kV and fell back to 90 Pa at 4 kV. This may also be caused by the accessional chemical reactions (such as hydrolysis reaction),[22–24] which affect the fluidic transportation. All the aforementioned results and analyses effectively demonstrate the high efficiency, capability, and controllability of the TEOP.

5. Demonstration of TEOP in Micro-Cooling and Liquid Mixing System

EOPs are widely used in biomedicine, chemical and electronic fields due to their advantages of no pulse, high stability, and easy integration. The EOF driven by the basic FS-TENG is inconsecutive, in order to obtain a continuous EOF, we use the rotating TENG (R-TENG). R-TENG has a radial interdigital electrode with 18 segments, which improves the output stability and continuity (Figure S14, Supporting Information). The charge accumulation rate across the EOP chip is constant (Figure S15, Supporting Information), and the curve is smooth, which is very suitable for the microfluidic system that requires a stable flow rate. Video S5, Supporting Information, demonstrated the continuous EOF driven by R-TENG. As shown in the three-dimensional schematic diagram in **Figure 4**a, we designed a micro-cooling system including a R-TENG, high-voltage rectifier and electro-osmotic heat dissipation chip. The ITO heating ring has a width of 0.5 mm that is driven by a DC source. The cooling processes are shown in Figure 4b. When the DC source is turned on, the heating ring rapidly heats up, then turn off the DC source and turn on TEOP, the coolant flowing (deionized water) through the heating ring can be clearly observed. When the temperature drops to room condition, the heating and cooling cycle is performed again. A detailed demonstration of heating and cooling cycles is shown in Video S6, Supporting
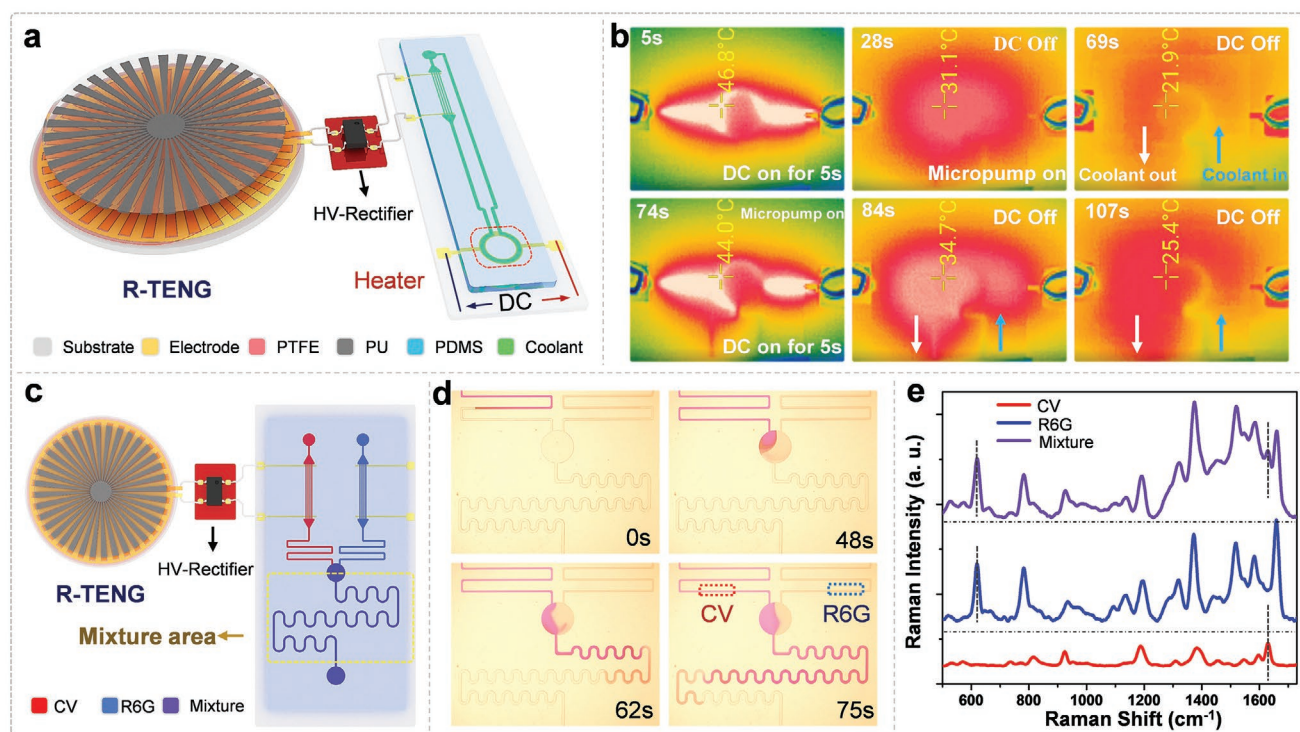
Figure 4. Demonstration of TEOP. a) 3D schematic diagram of a microheater cooling system based on rotational TENG driven continuous EOF. b) Thermal images of two heating and cooling cycle processes. c) Schematic diagram shows the application of TEOP in drug transportation and mixing. d) The process of drug transportation and mixing under an optical microscope. e) Raman spectrum of solutions in single and mixed channels.

Information. EOPs also have broad application prospects in drug delivery and mixing, so we designed an electroosmotic chip for drug delivery and mixing. As shown in Figure 4c, two TEOPs are applied to deliver and mix different drugs at the same time. Here, crystal violet (CV) and rhodamine 6G (R6G) were used for the demonstration. Figure 4d and Video S7, Supporting Information, clearly show the stable delivery and mixing process of the drugs. To prove the efficiency of the designed chip for drug mixing, Raman spectroscopy detection was performed at the single channel and the mixed channel. As shown in Figure 4e, the Raman peak of the mixture contains both the characteristic peaks of CV and R6G, indicating that the drug was fully mixed. These capabilities show that the TENG-driven EOP has excellent performance and provides a new choice for the drive of the EOP.

6. Conclusion and Outlook

We have demonstrated a motion-controlled micro-flow pump by TENG driven electroosmosis. Utilizing a basic F-S mode TENG, the performances and driven mechanism of TEOP were systematically studied and analyzed. The charge source feature of TENG could suppress the accessional reactions in EOF naturally. As a result, TENG driven EOP could produce ≈ 600 nL min^{-1} micro-flow with a Joule heat down to 1.76 J cm^{-3} nL^{-1} compared with ≈ 50 nL min^{-1} and 8.12 J cm^{-3} nL^{-1} for a traditional HV source driven EOP under 4 kV applied voltage. The minimum volume of 0.4 nL can be

precisely controlled by adjusting the sliding distance. The pump pressure up to 300 Pa was also quantitatively recorded using our designed unique testing platform. To reveal its capability in practical applications, a rotational TENG which driven continuous EOF was employed for micro-cooling and drug mixing processes. Under 0.5 r s^{-1} rotating speed, the temperature of the microheater can be reduced from 46.8 to 21.9 °C in 1 min, and two different liquids can be well mixed after 70 s. The advantages of TEOPs including economy, efficiency, portability, and safety, clearly present their potentials for the development and enrichment of motion-activated microsystems.

7. Experimental Section

Fabrication of the TEOP: The fabrication process of the TEOP can be divided into the preparation of the TENG component, rectifying circuit module and EOP chip. In this work, FS-TENG and R-TENG were both used in the experiments. For the FS-TENG, copper foil was first attached to a 150 mm × 100 mm acrylic sheet. The copper foil was then covered by a 50-µm-thick PTFE film after creating a gap of 5 mm to act as a stator. Next, an 80 × 70 mm polyurethane foam layer was attached to an acrylic sheet of the same size as the slider. For the R-TENG, a 2 mm thick PU sheet was shaped by a laser cutter to form a 1/18 annulus (inner diameter: 25 mm, external diameter: 150 mm), and then was stuck to one side of an acrylic substrate with the same configuration (thickness: 3 mm), acting as the slider. For the stationary electrode, use laser cutting to cut the substrate with acrylic into 1/18 annulus with a 0.5 mm pitch. Then, electrodes with complementary patterns had been deposited onto the disk by vacuum

coating. Two lead wires were connected respectively to the two sets of electrodes. A commercial FEP film (50 µm) was aligned onto the electrodes as a tribolayer. The high-voltage rectifier module consisted of four diodes in series. The electroosmotic chip was composed of conductive glass and microfluidic chip. Pasted Kapton on the ITO glass (7 Ω cm^{-2}), etched out the electrode area, and then washed the ITO mold outside the electrode area with hydrochloric acid to form the ITO electrode. Two ITO electrodes on the glass were 1 mm in width with the interval of 2 cm. (Figure S2, Supporting Information). The preparation process of the ITO heating ring was the same as that of the ITO electrode. PDMS and curing agent were poured on a patterned silicon wafer in a 10:1 configuration, baked at 80 °C for 3–5 h, and then reverse-molded to form a microfluidic chip. Finally, placed the ITO glass and the microfluidic chip in oxygen plasma for 4 min, and formed an electroosmotic chip after bonding (Figure S2, Supporting Information).

Measurement and Characterization: A field-emission scanning electron microscope (Hitachi SU8010) was used to characterize the morphologies of the nanostructured PTFE film. An optical microscope (Olympus SZX16, DP73) was used to measure the flow volume of the electroosmotic pump. The voltage and charge were recorded using a programmable electrometer (Keithley 6514). The software platform was constructed based on LabVIEW, which could realize real-time data acquisition control and analysis. Thermal imaging camera (IRay, T2S-A86) was used to record heat dissipation efficiency. The Raman measurements were performed on a Raman spectroscopy (iHR550, Horiba) at the excitation of 532 nm laser.

Supporting Information

Supporting Information is available from the Wiley Online Library or from the author.

Acknowledgements

Conflict of Interest

The authors declare no conflict of interest.

Data Availability Statement

The data that support the findings of this study are available from the corresponding author upon reasonable request.

Keywords

[1] H. L. Zhu, Z. Fohlerova, J. Pekarek, E. Basova, P. Neuzil, *Biosens. Bioelectron.* **2020**, *153*, 112041.

[2] S. R. Bazaz, A. Mashhadian, A. Ehsani, S. C. Saha, T. Krüger, M. E. Warkiani, *Lab Chip* **2020**, *20*, 1023.

[3] Q. R. Wu, J. F. Liu, X. H. Wang, L. Y. Feng, J. B. Wu, X. L. Zhu, W. J. Wen, X. Q. Gong, *Biomed. Eng. Online* **2020**, *19*, 1.

[4] V. Mohammad, S. M. Farhad, R. N. Elaheh, S. A. Mehdi, M. Shokouhimehr, *Ceram. Int.* **2020**, *46*, 1730.

[5] J. Knoška, L. Adriano, S. Awel, K. R. Beyerlein, O. Yefanov, D. Oberthuer, G. E. P. Murillo, N. Roth, I. Sarrou, P. Villanueva-Perez, M. O. Wiedorn, F. Wilde, S. Bajt, H. N. Chapman, M. Heymann, *Nat. Commun.* **2020**, *11*, 657.

[6] R. Novak, M. Ingram, S. Marquez, D. Das, A. Delahanty, A. Herland, B. M. Maoz, S. S. F. Jeanty, M. R. Somayaji, M. Burt, E. Calamari, A. Chalkiadaki, A. Cho, Y. Choe, D. B. Chou, M. Cronce, S. Dauth, T. Divic, J. Fernandez-Alcon, T. Ferrante, J. Ferrier, E. A. FitzGerald, R. Fleming, S. Jalili-Firoozinezhad, T. Grevesse, J. A. Goss, T. Hamkins-Indik, O. Henry, C. Hinojosa, T. Huffstater, K.-J. Jang, V. Kujala, L. Leng, R. Mannix, Y. Milton, J. Nawroth, B. A. Nestor, C. F. Ng, B. O'Connor, T.-E. Park, H. Sanchez, J. Sliz, A. Sontheimer-Phelps, B. Swenor, G. Thompson, G. J. Touloumes, Z. Tranchemontagne, N. Wen, M. Yadid, A. Bahinski, G. A. Hamilton, D. Levner, O. Levy, A. Przekwas, R. Prantil-Baun, K. K. Parker, D. E. Ingber, *Nat. Biomed. Eng.* **2020**, *4*, 407.

[7] W. L. Chou, P. L. Lee, C. L. Yang, W. Y. Huang, Y. S. Lin, *Micromachines* **2015**, *6*, 1249.

[8] P. Cui, S. Wang, *J. Pharmaceut. Biomed.* **2019**, *9*, 238.

[9] H.-Q. Chen, X.-Y. Wang, H. K. Bisoyi, L.-J. Chen, Q. Li, *Langmuir* **2021**, *37*, 3789.

[10] Y.-W. Shan, L.-Q. You, H. K. Bisoyi, Y.-J. Yang, Y.-H. Ge, K.-J. Che, S.-S. Li, L.-J. Chen, Q. Li, *Adv. Opt. Mater.* **2020**, *8*, 2000692.

[11] L. J. Chen, Y. N. Li, J. Fan, H. K. Bisoyi, D. A. Weitz, Q. Li, *Adv. Opt. Mater.* **2014**, *2*, 845.

[12] E. A. Sideris, H. C. de Lange, *Sens. Actuators, A* **2020**, *307*, 111915.

[13] M. J. Esplandiu, K. Zhang, J. Fraxedas, B. Sepulveda, D. Reguera, *Acc. Chem. Res.* **2018**, *51*, 1921.

[14] D. J. Laser, J. G. Santiago, *J. Micromech. Microeng.* **2004**, *14*, R35.

[15] L. Li, X. Y. Wang, Q. S. Pu, S. R. Liu, *Anal. Chim. Acta.* **2019**, *1060*, 1.

[16] S. M. Tian, W. L. Zhang, J. W. Shi, Z. X. Guo, M. Li, *Anal. Sci.* **2020**, *36*, 953.

[17] M. Gao, L. Gui, *Lab Chip* **2014**, *14*, 1866.

[18] F. Kitagawa, S. Wakagi, Y. Takegawa, I. Nukatsuka, *Anal. Sci.* **2019**, *35*, 889.

[19] H. J. Keh, Y. C. Liu, *J. Colloid Interface Sci.* **1995**, *172*, 222.

[20] A. E. Herr, J. I. Molho, J. G. Santiago, M. G. Mungal, T. W. Kenny, M. G. Garguilo, *Anal. Chem.* **2000**, *72*, 1053.

[21] X. C. Xuan, D. Q. Li, *J. Colloid Interface Sci.* **2005**, *289*, 291.

[22] S. J. Lee, T. J. Jeon, S. M. Kim, D. Kim, *Micromachines* **2016**, *7*, 109.

[23] L. Gui, C. L. Ren, *Anal. Chem.* **2006**, *78*, 6215.

[24] X. C. Xuan, B. Xu, D. Sinton, D. Q. Li, *Lab Chip* **2004**, *4*, 230.

[25] G.-J. Sun, J.-H. Yun, M.-W. Cheon, *Trans. Electr. Electron. Mater.* **2021**, *22*, 108.

[26] H. Haes Alhelou, P. Siano, *Appl. Sci.* **2021**, *11*, 274.

[27] M. Qiao, L. F. Liang, J. Zu, D, C, Hou, Z. J. L.i , B. Zhang, *Microelectron. Eng.* **2020**, *232*, 111416.

[28] Z. L. Wang, *Mater. Today* **2017**, *20*, 74.

[29] F.-R. Fan, Z.-Q. Tian, Z. L. Wang, *Nano Energy* **2012**, *1*, 328.

[30] Y. L. Zi, H. Y. Guo, Z. Wen, M.-H. Yeh, G. G. Hu, Z. L. Wang, *ACS Nano* **2016**, *10*, 4797.

[31] Z. Lin, B. Zhang, H. Guo, Z. Wu, H. Zou, J. Yang, Z. L. Wang, *Nano Energy* **2019**, *64*, 103908.

[32] D. K. Davies, *J. Phys. D. Appl. Phys.* **1969**, *2*, 1533.

[33] R. Lei, Y. X. Shi, Y. F. Ding, J. H. Nie, S. Y. Li, F. Wang, H. Zhai, X. Y. Chen, Z. L. Wang, *Energy Environ. Sci.* **2020**, *13*, 2178.

[34] C. S. Wu, A. C. Wang, W. B. Ding, H. Y. Guo, Z. L. Wang, *Adv. Energy Mater.* **2019**, *9*, 1802906.

[35] A. Y. Li, Y. L. Zi, H. Y. Guo, Z. L. Wang, F. M. Fernández, *Nat. Nanotechnol.* **2017**, *12*, 481.

[36] C. J. Li, Y. Y. Yin, B. Wang, T. Zhou, J. N. Wang, J. J. Luo, W. Tang, R. Cao, Z. Q. Yuan, N. W. Li, X. Y. Du, C. R. Wang, S. Y. Zhao, Y. B. Liu, Z. L. Wang, *ACS Nano* **2017**, *11*, 10439.

[37] J. Cheng, W. B. Ding, Y. L. Zi, Y. J. Lu, L. H. Ji, F. Liu, C. S. Wu, Z. L. Wang, *Nat. Commun.* **2018**, *9*, 3773.

[38] H. Y. Guo, J. Chen, L. F. Wang, A. C. Wang, Y. F. Li, C. H. An, J. H. He, C. G. Hu, V. K. S. Hsiao, Z. L. Wang, *Nat. Sustainability* **2020**, *4*, 147.

[39] C. Hughes, L.-H. Yeh, S. Z. Qian, *J. Phys. Chem. C* **2013**, *117*, 9322.

[40] S. H. Behrens, D. G. Grier, *J. Chem. Phys.* **2001**, *115*, 6716.

[41] Y. L. Zi, S. M. Niu, J. Wang, Z. Wen, W. Tang, Z. L. Wang, *Nat. Commun.* **2015**, *6*, 8376.